



The influence of specimen roughness on the rate of formation of U_3O_8 on UO_2 in air at 250°C

P. Taylor^{*}, R.J. McEachern, D.C. Doern, D.D. Wood

Atomic Energy of Canada Limited, Whiteshell Laboratories, Pinawa, Man., Canada R0E 1L0

Received 12 September 1997; accepted 24 March 1998

Abstract

Disks of sintered, unirradiated UO_2 fuel with different surface roughness were oxidized in air at 250°C. X-ray powder diffractometry was used to quantify the rate of U_3O_8 formation. The variation of the rate of U_3O_8 formation was most significant when the particle size of the polishing media was in the range 1–18 μm . The time to reach a given percentage conversion of UO_2 to U_3O_8 decreased by about a factor of 4 between the smoothest and roughest surfaces. This corresponds to an increase of about two orders of magnitude in the composite nucleation-and-growth rate constant, κ . This effect is attributed to a combination of increased surface area and increased surface density of nucleation sites, as well as a crystallographic orientation phenomenon. © 1998 Published by Elsevier Science B.V. All rights reserved.

1. Introduction

The two-step oxidation of UO_2 to U_3O_8 has been investigated intensively for over 40 years ([1] and references therein). One reason for the sustained interest is that the 36% volume increase,¹ associated with conversion of UO_2 to U_3O_8 , can cause swelling and splitting of previously defected fuel elements stored in air at elevated temperatures [3–5]. Therefore, it is important to understand the kinetics of U_3O_8 formation.

The surface roughness of a UO_2 specimen is one of many variables that can influence the kinetics of oxidation of UO_2 to U_3O_8 [1,6,7]. It is known that the rate of conversion to U_3O_8 is faster on a rough surface than a highly polished surface. The dependence of reaction kinetics on surface roughness can be attributed to a combination of factors, discussed in Section 3. Previous studies have only demonstrated this phenomenon qualitatively; here, we describe an attempt to quantify the effect of surface roughness on oxidation kinetics.

2. Experimental

Disk-shaped specimens of polycrystalline UO_2 , approximately 12 mm diameter and 2 mm thick, were prepared from pellets of unirradiated CANDU² fuel. First, a pellet was embedded in epoxy resin and the dished end was cut off, using a low-speed diamond saw, to produce a flat surface. This surface was then polished to the desired surface finish, using a Buehler Mini-met 1000 polishing device. The grinding and polishing media had the following particle sizes: 100, 45, 23 (400 grit), 17 (600 grit), 15, 7.5, 1.0, and 0.05 μm . The abrasive medium was SiC for the 400 and 600 grit finishes, and diamond for all others. Samples were polished for 5 min with each type of abrasive paper. Those samples polished finer than 400 grit were successively polished with progressively finer media starting with 400 grit, e.g., the 15 μm finish was achieved by polishing for 5 min with a 400-grit medium, then a further 5 min with 600-grit and finally another 5 min with 15 μm abrasive paste. After finishing this outer surface, the disk was then sawn from the pellet, and removed from the epoxy mount before

^{*} Corresponding author.

¹ The crystallographic and relative volumes of UO_2 , U_3O_7 , U_3O_8 , and various hydrated uranium oxides have been compiled by Taylor et al. [2].

² Canada Deuterium Uranium, registered trademark.

oxidation. Additional disks, with different surface finishes, could then be cut from the same pellet.

It should be noted that the particle size of the grinding media is not a direct measure of the amplitude of surface roughness. This point is illustrated in Fig. 1, which shows scanning electron microscope images of fractured cross sections of two UO_2 specimens, one ground to a 400-grit finish, and the other polished to a $0.05 \mu\text{m}$ finish. The amplitude of surface roughness in the former case is about $2 \mu\text{m}$, whereas the latter surface is essentially smooth and flat at the level of resolution of the microscope image.

Polished samples were oxidized in air at 250°C in a Blue M tube furnace with temperature control accurate to within 2°C . After heating, the samples were cooled to room temperature for analysis by X-ray powder diffractometry (XRD). Some specimens were heated only once, while others were re-heated after the XRD analysis and oxidized further; the heat-cool-analyse cycle was repeated until U_3O_8 powder began to spall from the sample surface. The total duration of oxidation varied between 24 and 200 h.

Samples were analyzed by XRD to determine the degree of surface conversion to U_3O_8 . The XRD data were

obtained directly from the specimen surfaces, using a Rigaku Rotaflex diffractometer equipped with a 12 kW rotating-anode Cu $\text{K}\alpha$ source and a diffracted-beam monochromator. The diffractometer scanning rate was $10^\circ (2\theta) \text{min}^{-1}$ for qualitative peak identification and $1^\circ (2\theta) \text{min}^{-1}$ for integrated intensity measurement of specific peaks.

3. Results and discussion

The XRD data were used to estimate the fraction, F , of UO_2 converted to U_3O_8 on the sample surface following the procedure described by Choi et al. [8]. For this purpose, the integrated intensity of the combined, overlapping $[2\ 0\ 0]$ and $[1\ 3\ 0]$ peaks was measured for U_3O_8 ($2\theta \sim 26.0^\circ$ with Cu $\text{K}\alpha$ radiation) and compared to the $[1\ 1\ 1]$ feature for $\text{U}_3\text{O}_7/\text{U}_4\text{O}_9$ ($2\theta \sim 28.5^\circ$)³. The fraction, F , is given by

$$F = \frac{I_{\text{U}_3\text{O}_8}}{I_{\text{U}_3\text{O}_8} + \alpha I_{\text{U}_3\text{O}_7}}, \quad (1)$$

where $I_{\text{U}_3\text{O}_8}$ is the integrated intensity of the U_3O_8 peak, $I_{\text{U}_3\text{O}_7}$ is the analogous intensity for the $\text{U}_3\text{O}_7/\text{U}_4\text{O}_9$ peak. The empirical factor (α) was previously determined to be 0.450 ± 0.033 , by XRD analysis of a series of identical UO_2 specimens, oxidized for various lengths of time [8].

The XRD analysis depth in our samples is approximately $1 \mu\text{m}$, i.e., 95% of the diffracted X-rays originate less than $0.9 \mu\text{m}$ below the surface for the XRD peaks used in the present study [8,10]. The formation of U_3O_8 on the surface of the 12 mm disks can thus be approximated by a two-dimensional nucleation-and-growth reaction mechanism, which can be described by the expression

$$F = 1 - \exp \left\{ -\frac{\pi\kappa t^3}{3} + \frac{\pi^2\kappa^2 t^6}{180} - \frac{11\pi^3\kappa^3 t^9}{45\,360} + \frac{5\pi^4\kappa^4 t^{12}}{399\,168} \right\}, \quad (2)$$

where t is the time and κ is a composite rate constant defined by

$$\kappa = K_g^2 K_n, \quad (3)$$

where K_n ($\text{s}^{-1} \text{m}^{-2}$) is the rate of nucleation per unit area of UO_2 and K_g (m s^{-1}) is the rate of linear (radial) growth of the circular nuclei of U_3O_8 [11].

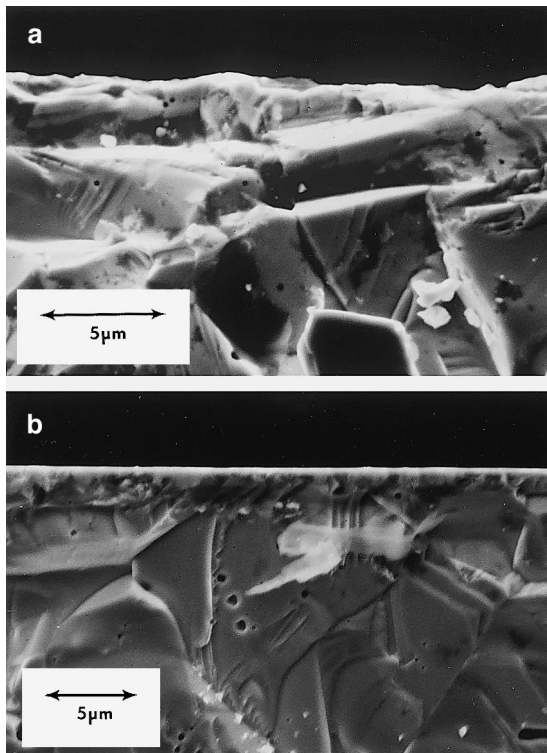


Fig. 1. Scanning electron micrographs of fractured cross sections of UO_2 specimens prepared with the following surface finishes: (a) 400-grit; (b) $0.05 \mu\text{m}$.

³ Oxidation of UO_2 to U_3O_8 proceeds through an intermediate oxygen-rich phase with a modified fluorite-type structure. The predominant phase with pure UO_2 starting material is usually U_3O_7 ; in the case of irradiated Light Water Reactor fuel, the intermediate oxidation product resembles $\gamma\text{-U}_4\text{O}_9$, but has a composition approaching $\text{UO}_{2.4}$ [1,9]. We use $\text{U}_3\text{O}_7/\text{U}_4\text{O}_9$ as a generic term to describe these intermediate products.

Table 1
Experimental XRD data, calculated values of F and the composite rate constant κ , and $T_{0.2}$, the estimated time to reach $F=0.2$

Polish	Time (h)	$I_{U_3O_8}$	$I_{U_3O_7}$	F	κ (h^{-3})	$T_{0.2}$ (h)
100 μm	96	671	5013	0.2293	2.8×10^{-7}	91
100 μm	24	51	10103	0.0111	7.4×10^{-7}	66
	48	495	9164	0.1072		
	96	1438	3445	0.4812		
45 μm	96	146	4949	0.0615	6.9×10^{-8}	146
45 μm	24	87	11722	0.0162	8.6×10^{-7}	63
	48	714	10283	0.1337		
	96	1878	3784	0.5245		
400 grit	96	683	4555	0.2499	3.2×10^{-7}	88
400 grit	24	0	14238	0.0000	7.6×10^{-8}	142
	48	23	7636	0.0066		
	72	231	12973	0.0381		
	96	378	7155	0.1051		
	120	551	6746	0.1536		
	148	888	6676	0.2282		
	172	1395	5649	0.3543		
	196	1539	5059	0.4033		
600 grit	96	1012	4717	0.3228	4.3×10^{-7}	80
600 grit	24	0	14737	0.0000	6.0×10^{-8}	153
	48	25	7784	0.0071		
	72	233	13356	0.0373		
	96	349	7470	0.0941		
	120	447	6546	0.1318		
	148	717	6898	0.1876		
	172	1142	6241	0.2891		
	196	1270	5623	0.3342		
15 μm	200	252	5725	0.0891	1.1×10^{-8}	268
15 μm	24	0	15035	0.0000	3.7×10^{-8}	180
	48	32	14407	0.0049		
	96	127	7804	0.0349		
7.5 μm	200	107	5358	0.0425	5.2×10^{-9}	346
7.5 μm	24	0	14824	0.0000	3.3×10^{-8}	187
	48	31	14157	0.0048		
	96	107	7604	0.0303		
1.0 μm	200	89	6279	0.0305	3.7×10^{-9}	388
1.0 μm	24	0	13960	0.0000	2.8×10^{-9}	425
	48	0	7604	0.0000		
	72	52	14030	0.0082		
	96	0	8539	0.0000		
	120	0	8012	0.0000		
	148	48	9190	0.0115		
	172	62	8829	0.0154		
	196	83	8398	0.0215		
0.05 μm	200	88	6134	0.0309	3.8×10^{-9}	384

Table 1 (Continued)

Polish	Time (h)	$I_{U_3O_8}$	$I_{U_3O_7}$	F	κ (h^{-3})	$T_{0.2}$ (h)
0.05 μm	24	0	13971	0.0000	2.8×10^{-9}	425
	48	0	7692	0.0000		
	72	0	14132	0.0000		
	96	0	8465	0.0000		
	120	0	8499	0.0000		
	148	51	9438	0.0119		
	172	63	8985	0.0153		
	196	81	8348	0.0211		

Table 1 shows measured values of $I_{U_3O_7}$ and $I_{U_3O_8}$ together with calculated values of F and κ , for each UO_2 specimen. The values of κ were calculated by minimizing the sum of the squares of deviations between calculated and experimentally observed values of F according to Eq. (2). The origin was included as a data point in the determination of κ values.

In Fig. 2, the calculated values of κ are plotted as a function of the particle size of the polishing agents used to prepare the various specimens. For each value of κ in Table 1, the time required to achieve an F value of 0.2 was calculated. These times are plotted as a function of the particle size of the polishing agents in Fig. 3, which clearly shows that U_3O_8 was formed more rapidly on rough than highly polished surfaces. The time to achieve a given fraction of surface conversion to U_3O_8 was about four times longer on the smoothest UO_2 surfaces than the roughest ones. The magnitude of the surface-roughness effect is consistent with that reported previously [7] for U_3O_8 formation on 400-grit, 15 and 3 μm surfaces at 200°C to 300°C.

Examination of data from 11 different oxidation tests on UO_2 disks with 400-grit finish, originating from five

different fuel pellets, indicated that the uncertainty (95% confidence limit) in individual values of κ is about one order of magnitude or 2.3 natural log units, compared with the range of about 5 natural log units between κ values for rough and polished specimens in Fig. 2. The variability between different pellets was greater than that between different disks cut from the same pellet. The sources of this variability are not well understood; one likely factor is local variation in density and grain size within individual pellets. Results are also sensitive to the accuracy of temperature control [1,7,11].

The relationship between κ and surface roughness is not linear. The experimentally determined values of κ are essentially independent of the particle size of the polishing agent when the latter is either very fine ($\leq 1 \mu m$) or coarse (18–100 μm). For polishing media with a particle size between 1 and 18 μm , the κ values increase with increasing particle size; we attribute this to an increase in K_n , the rate constant for nucleation.

The acceleration of U_3O_8 formation on UO_2 with increasing roughness can be attributed to a combination of at least three factors. First, with increasing roughness, the *microscopic* surface area increases, and therefore the *geometric* (macroscopic) surface density of nucleation sites will be expected to increase in proportion. Second, and probably more important, a rough surface will have sharp edges and points that are likely to promote nucle-

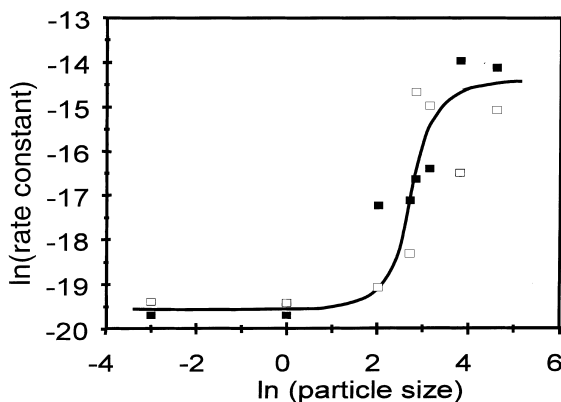


Fig. 2. Calculated values of the composite rate constant κ as a function of the particle size of the polishing medium used to prepare the UO_2 specimens. Open symbols represent calculated values of κ from single oxidation tests; closed symbols represent fitted values from sequential oxidation tests.

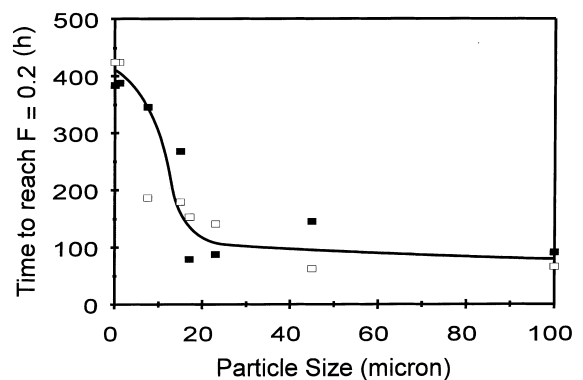


Fig. 3. Calculated times for surface oxidation to proceed to values of $F = 0.2$; symbols have the same meanings as in Fig. 2.

ation of U_3O_8 , thus increasing the *microscopic* surface density of nucleation sites. Previous studies have shown that the nucleation sites of U_3O_8 on polished UO_2 disks, at temperatures below 300°C, are sparsely distributed and tend to be localized at surface irregularities or areas of locally high porosity [7]. The localized, patchy distribution of U_3O_8 nucleation sites is also often apparent by visual inspection of oxidized UO_2 specimens. Thus, the rate of U_3O_8 formation is likely independent of the polishing-medium particle size when it is less than $\approx 1 \mu\text{m}$ because the rate of nucleation has reached an inherent value related to the density of macroscopic flaws in the sintered UO_2 . The independence of κ on grinding-medium particle size for very coarse media ($>18 \mu\text{m}$) indicates that the surface state is essentially the same for any media that are much coarser than the UO_2 grain size ($\sim 10 \mu\text{m}$).

The third factor affecting the rate of U_3O_8 formation is a more subtle, crystallographic nuance [7,12]. Nearly all of the 36% expansion associated with the conversion of UO_2 to U_3O_8 is accommodated in the $\langle 1\ 1\ 1 \rangle$ crystallographic direction of the original UO_2 , which becomes the $0\ 0\ 1$ direction (c axis) of U_3O_8 . Thus, grains in which a $\langle 1\ 1\ 1 \rangle$ axis lies normal to the surface are oxidized preferentially. With a polished surface, the $0\ 0\ n$ XRD peaks for U_3O_8 are thus enhanced (the peaks are generated by those grains that are oriented with a specific crystallographic plane parallel to the geometric surface). On a rough surface, individual grain faces are generally not parallel to the geometric surface of the sample, therefore the preferred orientation effect in the XRD pattern is diminished. On a surface that is rough on a sub-granular scale, the probability that part of the surface of a given grain is normal to $\langle 1\ 1\ 1 \rangle$ will also be greater than in the case of a highly polished surface. Sintered UO_2 pellets themselves do not display any preferred orientation, i.e., the relative intensities of the XRD peaks for the unoxidized disks were always close to the theoretical values for UO_2 .

4. Conclusions

The rate of formation of U_3O_8 on disks of sintered, unirradiated UO_2 by air oxidation depends on surface roughness, among other factors. The effect of surface roughness on the rate of U_3O_8 formation is most significant when the particle size of the polishing media is in the range 1–18 μm . The increase in the rate of U_3O_8 formation with increased surface roughness can be

attributed to a combination of increased surface area, increased surface density of nucleation sites, and a preferred-orientation phenomenon related to the crystallographic relationship between the UO_2 precursor and U_3O_8 product phases. The time to reach a given degree of conversion of UO_2 to U_3O_8 varies by about a factor of four between the roughest and smoothest UO_2 specimen surfaces investigated. Data obtained for the oxidation of rough surfaces can therefore be considered conservative when used judiciously to calculate U_3O_8 formation rates on UO_2 fuel, i.e., the calculations are unlikely to underestimate the rate of U_3O_8 formation. It should also be noted that the roughness of a fuel surface may vary in the course of oxidation when U_3O_8 powder spalls from the surface and exposes fresh material to oxidation.

Acknowledgements

The authors appreciate critical review of a draft manuscript by D.W. Shoesmith and W.H. Hocking. We also thank D.G. Owen for the scanning electron micrographs. This work was funded by AECL as part of the Underlying Chemistry research program.

References

- [1] R.J. McEachern, P. Taylor, J. Nucl. Mater. 254 (1998) 87.
- [2] P. Taylor, D.D. Wood, A.M. Duclos, D.G. Owen, J. Nucl. Mater. 168 (1989) 70.
- [3] D.G. Boase, T.T. Vandergraaf, Nucl. Technol. 32 (1977) 60.
- [4] R.E. Einziger, J.A. Cook, Nucl. Technol. 69 (1985) 55.
- [5] J. Novak, I.J. Hastings, E. Mizzan, R.J. Chenier, Nucl. Technol. 63 (1983) 254.
- [6] P.A. Tempest, P.M. Tucker, J.W. Tyler, J. Nucl. Mater. 151 (1988) 251.
- [7] P. Taylor, D.D. Wood, A.M. Duclos, J. Nucl. Mater. 189 (1992) 116.
- [8] J.-W. Choi, R.J. McEachern, P. Taylor, D.D. Wood, J. Nucl. Mater. 230 (1996) 250.
- [9] L.E. Thomas, R.E. Einziger, H.C. Buchanan, J. Nucl. Mater. 201 (1993) 310.
- [10] P. Taylor, E.A. Burgess, D.G. Owen, J. Nucl. Mater. 88 (1980) 153.
- [11] R.J. McEachern, J.-W. Choi, M. Kolar, W. Long, P. Taylor, D.D. Wood, J. Nucl. Mater. 249 (1997) 58.
- [12] G.C. Allen, P.A. Tempest, J.W. Tyler, Philos. Mag. B 54 (1986) L67.